RESEARCH ARTICLE

Investigation of eluted characteristics of fulvic acids using differential spectroscopy combined with Gaussian deconvolution and spectral indices

Tingting Li[1] · Fanhao Song[1,2] · Jin Zhang[3] · Shasha Liu[1] · Weiying Feng[1] · Lingling Zuo[4] · Jia Pu[2] · Baoshan Xing[5] · John P. Giesy[1,6] · Yingchen Bai[1]

Abstract

The characteristics of subfractions of soil fulvic acid (FA_3, FA_5, FA_7, FA_9, and FA_{13}) using stepwise elution from XAD-8 resin with pyrophosphate buffers were investigated by differential absorption spectroscopy (DAS) and differential fluorescence spectroscopy (DFS) combined with mathematical deconvolution and spectral indices. The log-transformed absorbance spectra (LTAS) exhibited three regions for both acidic-buffer-eluted subfractions (AESF) and neutral-buffer-eluted subfraction (NESF) and four regions for basic-buffer-eluted subfractions (BESF) according to the differences in spectral slopes. The DAS spectra of FA subfractions were closely fitted with seven Gaussian bands with maxima location at 199.66, 216.18 ± 1.50, 246.20 ± 3.85, 285.22 ± 7.26, 345.64 ± 5.30, 389.27, and 307.37 nm, respectively ($R^2 > 0.993$). The content of salicylic-like and carboxyl groups in FA subfractions decreased, while the phenolic chromophore increased with elution sequence. From the 11 spectral indices, AESF had greater molecular weight, condensation, polymerization, hydroxyl radical production, humification degree, and terrigenous contribution, as well as contained more conjugated aromatic structures and less N-containing groups than NESF and BESF. The humification degree and humic characters of FA subfractions were closely associated to the aromaticity, molecular condensation, and DOM–metal-bound functional groups. The proper separation of FA into subfractions is beneficial for reducing its complexity and heterogeneity, which helps us to further explore its chemical properties and interactions with various contaminants in soil environments.

Keywords UV–Vis · Gaussian bands · Chromophores · EEM · Humification degree

---

Tingting Li and Fanhao Song contributed equally to this work.

✉ Yingchen Bai
  baiyc@craes.org.cn

1 State Key Laboratory of Environmental Criteria and Risk Assessment, Chinese Research Academy of Environmental Sciences, Beijing 10012, China

2 College of Water Sciences, Beijing Normal University, Beijing 100875, China

3 School of Environmental and Safety Engineering, Changzhou University, Jiangsu 213164, China

4 School of Management, China University of Mining and Technology, Beijing 221116, China

5 Stockbridge School of Agriculture, University of Massachusetts, Amherst, MA 01003, USA

6 Department of Biomedical and Veterinary Biosciences and Toxicology Centre, University of Saskatchewan, Saskatoon, SK S7N 5B3, Canada

Abbreviations

AESF	Acidic-buffer-eluted subfractions
BESF	Basic-buffer-eluted subfractions
BI	Biological index
DAS	Differential absorption spectroscopy
DFS	Differential fluorescence spectroscopy
DOM	Dissolved organic matter
EEM	Excitation–emission matrix
FA	Fulvic acid
FI	Fluorescence index
HA	Humic acid
HIX	Humification index
LTAS	Log-transformed absorbance spectra
NESF	Neutral-buffer-eluted subfraction

Introduction

Fulvic acid (FA) is a complicated mixture of macromolecular organic compounds with various building blocks and functional groups occurring in water, soil, and sediment environments (Bai et al. 2015; Song et al. 2017a; Yue et al. 2017; Zhang et al. 2017). The chemical and structural heterogeneity of FA makes it difficult to understand and predict its effects on the mobilization and bioavailability of metals, polycyclic aromatic hydrocarbons, and other contaminants (Bai et al. 2015; Dai et al. 2006; Li et al. 2020b). Reduction of heterogeneity by separating FA into subfractions will be beneficial to explore the FA properties and evaluate the interactions with chemical species (Dai et al. 2006; Kalbitz et al. 1999). Additionally, the stepwise elution method combined with XAD resin has been successfully used to separate the soil FA into five subfractions in our recent studies (Bai et al. 2015; Song et al. 2017b). The differences of compositions and structures among FA subfractions were observed; for example, the content of carbon and oxygen elements in subfractions increased and decreased with elution sequence, respectively (Bai et al. 2015). The number-averaged and mass-averaged molecular mass of our FA subfractions also decreased from 3814 ± 21 to 1754 ± 28 Da and from 4432 ± 10 to 3369 ± 90 Da with elution sequence, respectively (Bai et al. 2015). Although the compositional characteristics of FA subfractions have been briefly investigated, more comprehensive differences among FA subfractions have not been fully studied.

The ultraviolet and visible (UV–Vis) and three-dimensional excitation–emission matrix (EEM) spectroscopy have been widely applied to characterize the FAs and humic acids (HA) due to their advantages of simple operation, low sample dosage, and high sensitivity (Albrecht et al. 2011; Fuentes et al. 2006; He et al. 2016; Miao et al. 2019; Pan et al. 2017; Peng et al. 2014). The original UV–Vis and EEM spectra are featureless and difficult to quantitatively identify the differences among FAs, humic acids, or dissolved

organic matters (DOM). Therefore, in order to obtain a more comprehensive representation of FA properties, two more recent methods, differential absorption spectroscopy (DAS) and differential fluorescence spectroscopy (DFS), are developed based on the UV–Vis and EEM spectra. Compared to the broad and featureless features of UV–Vis spectra, the DAS has advantages in reflecting the subtle changes and identifying the overlapping bands in spectra (Dryer et al. 2008; Yan et al. 2014). The Gaussian fitting model has proved to be a successful method to quantitatively distinguish the overlap and "hidden" peaks (Li et al. 2020a; Song et al. 2019a). Therefore, the numeric deconvolution of DAS by Gaussian fitting model can highlight the spectral features of chromophores in FAs or other organic matters (Yan et al. 2013a, 2016). For example, DAS combined with Gaussian fitting model is widely used to explore the interactions of metals (e.g., Ca^{2+}, Mg^{2+}, Fe^{3+}) with standard DOM, finding that the DAS could reveal the nature and extent of DOM–metal interactions (Yan et al. 2013a, 2015; Yan and Korshin 2014). Moreover, the DAS combined with Gaussian fitting model was also successfully utilized to explore the effects of ionic strength on the chromophores of DOM from autochthonous and allochthonous aquatic systems (Gao et al. 2015b). The DFS could eliminate fluorescence of nonreactive matters and allow examination of subtle changes in EEMs of samples of interest by directly subtracting the fluorescence spectra of reference samples (Song et al. 2018; Yan et al. 2013b). For example, the DFS had been successfully performed to estimate the influence of pH on the fluorescence of Suwannee River and Nordic Reservoir DOM (Yan et al. 2013b). However, the new spectral analyses, DAS and DFS, combined with mathematical deconvolution technique have not been integrated to characterize FA subfractions and estimate their dynamic changes with elution sequence. Recently, the adsorption and fluorescence indices have been applied to investigate the chemical composition, humification degree, fluorescent quantum yield, aromaticity, and other characteristics of FAs, which have broaden the understanding of DOM to a large extent (Birdwell and Valsaraj 2010; Fuentes et al. 2006; Helms et al. 2008; Li and Hur 2017; Yu et al. 2011; Xu et al. 2018a, b). For example, the differential slopes in the range of 350–400 nm ($\Delta S_{350–400}$) from DAS were utilized to evaluate the amount of functional groups bound to metals in DOM or FAs (Yan et al. 2013c). Additionally, the fluorescence index (FI), biological index (BI), and humification index (HIX) derived from EEMs can indicate the aromaticity, terrigenous contribution, and humic character of DOM or FAs (Birdwell and Engel 2010; Birdwell and Valsaraj 2010; Huguet et al. 2009; Pan et al. 2017; Song et al. 2019b). However, the correlations of various spectral indices of DOM or FAs are still not very clear, especially for the spectral indices of FA subfractions with specific differences.

Five subfractions of soil FA were obtained by stepwise elution from XAD-8 resin coupled with pyrophosphate buffers

with different pH values in our previous study (Bai et al. 2015). In this study, we revisited the FA subfractions with different new perspectives, and the objective of this study mainly focused on the eluting-dependent changes of subfractions using novel differential spectroscopy (i.e., DAS and DFS) combined with Gaussian deconvolution. In addition, based on the data from differential spectroscopy, an integrated index evaluation and correlation were also presented to further investigate the variations in characteristics (e.g., humification degree) of subfractions during the fractionation process.

Materials and methods

Isolation and fractionation of FA subfractions

Soil sample was collected from Jiufeng Mountain Forest, Beijing, China (N 39° 54′, E 116° 28′). The detailed information on isolation of soil FA, as well as the separation of subfractions of soil FA, has been previously reported (Bai et al. 2015). In brief, the soil samples were air-dried and then passed through a 2-mm sieve. The soil FA was extracted and purified according to the detailed procedures recommended by the International Humic Substances Society. Purified soil FA was redissolved in deionized water by adjusting the pH = 1.0 and reloaded to XAD-8 resin. Different stepwise eluents were prepared by the use of pyrophosphate buffers with initial pH of 3, 5, 7, 9, and 13, respectively. After elution with each buffer, the eluate was acidified and purified by the use of XAD-8 resin and H$^+$-saturated cation exchanged resin (Bio-Rad, Richmond, CA). Finally, the soil FA was successfully fractioned into five subfractions, named as FA$_3$, FA$_5$, FA$_7$, FA$_9$, and FA$_{13}$ (FA$_3$ and FA$_5$: acidic-buffer-eluted subfractions, AESF; FA$_7$: neutrual-buffer-eluted subfraction, NESF; FA$_9$ and FA$_{13}$: basic-buffer-eluted subfractions, BESF). In addition, the UV–Vis absorbance at 650 nm was used to quantify the concentration of subfractions during stepwise elution processes (Bai et al. 2015). The absorbance at 650 nm of eluent from ending elution with each sodium pyrophosphate buffer was closed to zero to ensure maximum isolation. The suitable selection of pH values of sodium pyrophosphate buffers could minimize the impacts of mixture of neighboring buffers. Moreover, several processes were used to minimize the experimental errors: (1) the purified FA was used to reduce the errors due to impure samples; (2) each of the purified FA subfractions was dissolved in the same background solution with KClO$_4$ (pH = 7.0 ± 0.05); and (3) the pH values of the subfraction solutions were finely adjusted. The errors of UV–Vis and EEM measurements were also very small according to the conditional experiments. All chemicals were analytical reagent grade unless otherwise noted and solutions were prepared with Milli-Q water, and then filtered through 0.45 μm glass fiber membrane filters before analysis.

UV–Vis spectra measurements

Solutions of FA subfractions were prepared at 10.0 mg L^{-1} with 0.05 mol L^{-1} KClO$_4$ as ionic strength. The KClO$_4$ ionic strength with low concentration was considered to have no effects on the fluorescence intensities of organic matters (Fu 2014; Mobed et al. 1996). Solutions of FA subfractions were adjusted to approximately pH 7.0 ± 0.05 by injecting submicroliter amounts of HClO$_4$ or NaOH with N$_2$ atmosphere at 25 ± 1 °C to avoid the pH effects on the UV–Vis spectra of subfractions. The UV–Vis spectra of FA subfractions were measured by using an ultraviolet–visible spectrophotometer (Agilent-8453) with a 1-cm quartz cuvette. The UV–Vis scan wavelengths ranged from 200 to 425 nm with 1 nm interval. Log-transformed absorbance spectra (LTAS) were calculated by natural logarithm transforming the absorbance of UV–Vis spectra (Yan et al. 2013c). SUVA$_{254}$ was defined as the UV–Vis absorbance at 254 nm that was normalized to subfraction concentration. Additionally, the E_{300}/E_{400} and $A_{240–400}$ represented the ratio of absorbance at 300 nm to that at 400 nm, and the integral area was calculated from 240 to 400 nm, respectively (He et al. 2011; Zhu et al. 2017). $S_{350–400}$ was the spectral slope parameter, which was the rate of changes at wavelength range of 350–400 nm in LTAS of FA subfractions (Yan et al. 2016; Xu et al. 2018a, b).

Deconvolution of DAS

The DAS was established based on original UV–Vis spectra of FA subfractions. A_{FA_i} and A_{ref} were the UV–Vis absorbance of the interest FA$_i$ (i = 3, 5, 7, and 9) and the reference FA$_{13}$, respectively. $A_{FA_i-blank}$ and $A_{ref-blank}$ were the UV–Vis absorbance of corresponding blanks of the interest FA$_i$ and reference FA$_{13}$, respectively (Eq. (1)) (Janot et al. 2010).

$$DA_{FA_i} = \frac{1}{l}\left(\frac{A_{FA_i}-A_{FA_i-blank}}{C_{FA_i}} - \frac{A_{ref}-A_{ref-blank}}{C_{ref}}\right) \quad (1)$$

Where C_{FA_i} and C_{ref} are the concentrations of interest FA$_i$ and reference FA$_{13}$, respectively, and l is the cell length. The $\Delta A_{254}/A_{254}$, $\Delta S_{350–400}$, and $\Delta LnA(350)$ are the relative changes of DAS absorbance at 254 nm, the differential slopes in DAS range of 350–400 nm, and the differential log-transformed absorbance at 350 nm, respectively (Gao et al. 2015b; Li and Hur 2017).

The Gaussian fitting model was processed to determine the existence and contributions of distinct bands in the UV–Vis spectra. The different bands described by Gaussian shape and photon energy (measured in eV) could be established with Eq. (2) (Yan and Korshin 2014; Yan et al. 2013c).

$$E(\text{eV}) = E_{oi}(A_{oi}) = \frac{1240}{\lambda} \qquad (2)$$

Gaussian bands were characterized by the location of maximum (E_{oi}), intensity at $E(\text{eV}) = E_{oi}(A_{oi})$, and width ($W_i$) of bands. The differential spectra ($DA(E)$) could be calculated with electron volt as unit (Eq. (3)) (Yan et al. 2013a; Yan and Korshin 2014).

$$DA(E) = \sum_i DA_{oi} \exp\left[-\left(\frac{E-E_{oi}}{\sqrt{2}W_i}\right)^2\right] \qquad (3)$$

The Gaussian fitting model for DAS curves was conducted by the use of OriginPro 9.1 and PeakFit 4.0 software in this study.

EEM measurements and DFS calculation

The EEMs of FA subfractions were measured by the use of a fluorescence spectrometer (Hitachi F-7000, Tokyo, Japan) with a 1-cm path-length quartz cuvette at 25 ± 1 °C. Before the EEM measurements, the pH value of each solution of FA subfractions was adjusted to 7.0 ± 0.05 by injecting submicroliter amounts of $HClO_4$ or NaOH solutions. The scanning ranges of excitation wavelength (Ex) and emission wavelength (Em) were 200–450 and 250–550 nm, respectively. The slit widths of both excitation and emission were 5 nm, and the scanning speed was set at 2400 nm min^{-1}. The blank EEMs of $KClO_4$ at 0.05 mol L^{-1} were subtracted from the EEMs of FA subfractions. Interpolation was used to regulate the Rayleigh and Raman scatters (Chen and Kenny 2012; Yu et al. 2010). The D-EEM was conducted to distinguish the EEM changes with elution sequences according to previous studies (Eq. (4)) (Fu 2014; Parker and Rees 1960; Song et al. 2018; Yan et al. 2013b).

$$\text{D-EEM} = -\frac{1}{1}\left(\frac{EEM_{FA_i} - EEM_{FA_i-\text{blank}}}{C_{FA_i}} - \frac{EEM_{\text{ref}} - EEM_{\text{ref-blank}}}{C_{\text{ref}}}\right) \quad (4)$$

Where D-EEM is the differential EEMs of interest FA_i ($i = 3, 5, 7,$ and 9); EEM_{FA_i} and EEM_{ref} are the EEMs of the interest FA_i and the reference FA_{13}, respectively; $EEM_{FA_i-\text{blank}}$ and $EEM_{\text{ref-blank}}$ are the EEMs of corresponding blanks of the interest FA_i and reference FA_{13}, respectively (Song et al. 2018).

FI was calculated as intensity ratio at emission 450 nm to that at 500 nm with a fixed excitation at 370 nm (Mcknight et al. 2001; Praise et al. 2018). The average fluorescence intensity per unit of average UV absorbance (AFI/UV) was established as the ratio of the average fluorescence intensity of Ex/Em at 200–400/250–500 nm to the average UV–Vis absorbance at 200–400 nm (Xiao et al. 2016). BI was obtained from the intensity ratio at emission 380 to 430 nm, using a fixed excitation at 310 nm (Birdwell and Engel 2010). In addition, HIX was obtained from the intensity ratio of sum emission at 435–480 nm to that at 300–345 nm, following a fixed excitation at 254 nm (Mielnik and Kowalczuk 2018; Ohno et al. 2007).

Results and discussion

DAS analysis of FA subfractions

The decreasing absorbance in the UV–Vis spectra of five FA subfractions with increasing wavelengths were observed and reported in a previous literature (Bai et al. 2015). The UV–Vis spectra of FA subfractions were featureless and change little with elution sequence; therefore, the LTAS were established according to zero-order absorbance spectra to further estimate the properties of FA subfractions (Fig. 1a). The LTAS of both AESF and NESF exhibited decreasing characteristics with three regions (i.e., regions at ~ 200–230, ~ 230–350, and ~ 350–425 nm) with somewhat different spectral slopes (Fig. 1a). The slope changes of LTAS of BESF were more evident than those of AESF and NESF, showing four regions at about ~ 200–230, ~ 230–280, ~ 280–325, and ~ 325–425 nm in LTAS (Fig. 1a). The evident LTAS changes of BESF could be supported by the first-order derivative of log-transformed absorbance of FA subfractions (Fig. S4). In detail, one strong shoulder at approximate 275–325 nm was observed in LTAS of both FA_9 and FA_{13} (Fig. 1a). Different slopes of regions in LTAS of each subfraction were associated with the variations of chromophore and/or molecule conformations (Yan et al. 2013c). This phenomenon was also reported by Yan et al. (2013a), who focused on the copper binding of Suwannee River FA obtained from the International Humic Substances Society (Yan et al. 2013a).

The DASs of interest FA subfractions (i.e., FA_3–FA_9) were calculated with FA_{13} as the reference and defined as DFA_3–DFA_9, respectively (Fig. 1b). The DASs of FA_3–FA_9 exhibited two to three specific peaks that evolved with stepwise elution (Fig. 1b). Similar patterns of DFA_3–DFA_7 showed three notable features, namely (1) the broadest and strongest peak located at around 250 nm, (2) two shoulders with a maximum at around 215 and 295 nm, and (3) the maximum absorbance with the order of $DFA_3 > DFA_5 > DFA_7$ (Fig. 1b). Moreover, the DFA_9 showed one narrow shoulder with a maximum close to 215 nm and one broad and strong peak with a maximum centered around 280 nm (Fig. 1b). The distinguished DAS peaks with similar locations were also observed by other researchers, who investigated the protonation behaviors of FAs and HAs by the use of spectrophotometric titrations (Gao et al. 2015b; Yan et al. 2013a; c). The different peaks in DFA_3–DFA_9 might indicate the presence of dissimilar UV–Vis chromophores in FA_3–FA_9 (Gao et al. 2015a; Janot et al. 2010). For examples, the DAS peaks with wavelengths at around
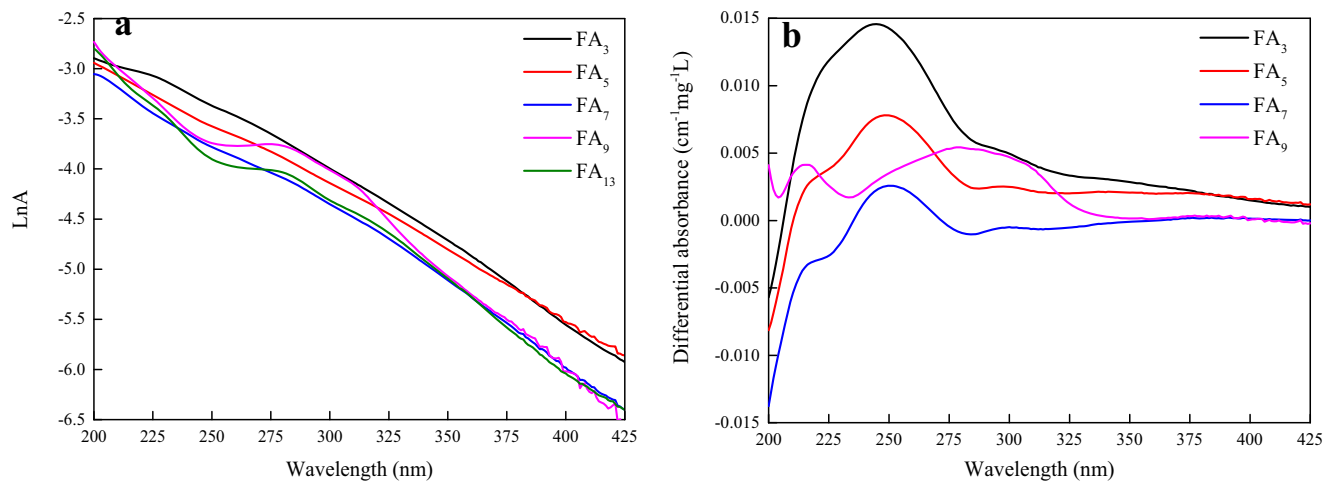
Fig. 1 Log-transformed absorbance spectra (**a**) of FA subfractions and differential absorbance spectra (**b**) of FA$_3$–FA$_9$ (FA$_{13}$ as reference)

280 nm were related to carboxylic groups (Chen et al. 2019; Dryer et al. 2008). Therefore, the presence of different peaks among DFA$_3$–DFA$_9$ should be studied further by the use of deconvolution of DAS.

Deconvolution of DAS of subfractions

The presence and contributions of distinct bands in DAS for interest FA subfractions were identified by the use of the Gaussian fitting model (Fig. 2). The experimental and model DFA$_3$–DFA$_9$ showed a value very close to 1 corresponding to a low variance ($R^2 > 0.993$) (Fig. 2, Table 1). Seven Gaussian bands were distinguished in DFA$_3$–DFA$_9$ (Fig. 2, Table 1). The maxima of Gaussian bands were operationally referred to as A0–A6, which are located at 6.20 eV (200 nm), 5.74 ± 0.04 eV (216.18 ± 1.50 nm), 5.09 ± 0.08 eV (246.20 ± 3.85 nm), 4.35 ± 0.11 eV (285.22 ± 7.26 nm), 3.59 ± 0.06 eV (345.64 ± 5.30 nm), 3.19 ± 0.01 eV (389.27 ± 0.79 nm), and 4.03 eV (307.37 nm), respectively (Table 1). Moreover, the widths of A0–A6 were 1.16, 7.12 ± 0.97, 16.78 ± 3.85, 25.23 ± 5.20, 29.50 ± 6.72, 17.43 ± 0.52, and 10.13 nm, respectively (Table 1). The A0 and A1 bands located at energies > 5.5 eV (wavelengths < 220 nm) were difficult to estimate their locations and characteristics due to the presence in various cases of spectroscopic interferences, such as inorganic ions (Yan and Korshin 2014). Therefore, only the bands located at energies < 5.5 eV or wavelengths > 220 nm (i.e., A2–A6) were discussed henceforth in this study.

The features of A2–A6 in DFA$_3$–DFA$_9$ had some limited similarities with the features of Gaussian bands from protonation-dependent DAS of Suwannee River FA and FA model species (e.g., sulfosalicylic acid, tannic acid, and salicylic acid) (Dryer et al. 2008; Yan et al. 2013a). In detail, the A2 in DFA$_3$–DFA$_7$ exhibited stronger spectral shapes than A3–A5 in DFA$_3$–DFA$_7$, while the A3 in DFA$_9$ contributed most to the spectral shape (Fig. 2). According to previous

literatures, the Gaussian bands A2, A3, A4, A5, and A6 were related to salicylic-type groups, carboxyl groups, tannic-type groups, phenolic chromophore groups, and phenolic hydroxyl groups, respectively (Dryer et al. 2008; Janot et al. 2010; Yan et al. 2013c). Although the locations of Gaussian bands A3 for DFA$_3$–DFA$_9$ had a relatively larger wavelength range (285.22 ± 7.26 nm), all Gaussian bands A3 could represent the carboxyl groups according to previous studies (Chen et al. 2019; Dryer et al. 2008). The positions of the maxima of A2–A6 did not undergo significant changes (e.g., A2–A4 in DFA$_3$–DFA$_7$), while the intensities, widths, and areas of these Gaussian bands were slightly changed with elution sequence (Figs. 2 and 3, Table 1). The A2 areas (0.57–0.69) for DFA$_3$–DFA$_7$ were much greater than that (0.04) for DFA$_9$, showing decreases as the elution sequence (Fig. 3). Meanwhile, the similar A3 areas (0.40–0.48) for DFA$_3$–DFA$_7$ were about 2.5 times that (0.18) for DFA$_9$ (Fig. 3). Therefore, the salicylic-like and carboxyl groups were dominant in FA$_3$–FA$_7$ subfractions that were eluted by acidic and neutral elution buffers. In addition, the salicylic-like and carboxyl groups decreased sharply in subfractions with alkaline buffer elution. These phenomena were attributed to the ionization of carboxylic groups in FA subfractions at acidic conditions. The FA subfractions containing more carboxylic groups became sufficiently hydrophilic to be desorbed from the hydrophobic XAD-8 resin. The possible decrease of carboxyl groups with elution sequence was also obtained by ^{13}C-NMR analysis (Bai et al. 2015). In addition, the A4 areas for DFA$_3$–DFA$_7$ showed decreases from 0.39 to 0.18 with elution sequence and then disappeared for DFA$_9$ (Fig. 3). The A5 areas for both DFA$_5$ and DFA$_7$ with 0.04 to 0.07 were similar (Fig. 3). These results might indicate that the tannic-type groups were decreasing with elution sequence, and the contents of phenolic chromophore were similar between DFA$_5$ and DFA$_7$. The band of A6 related to phenolic hydroxyl groups only appeared in DFA$_9$, indicating greater content of phenolic hydroxyl groups
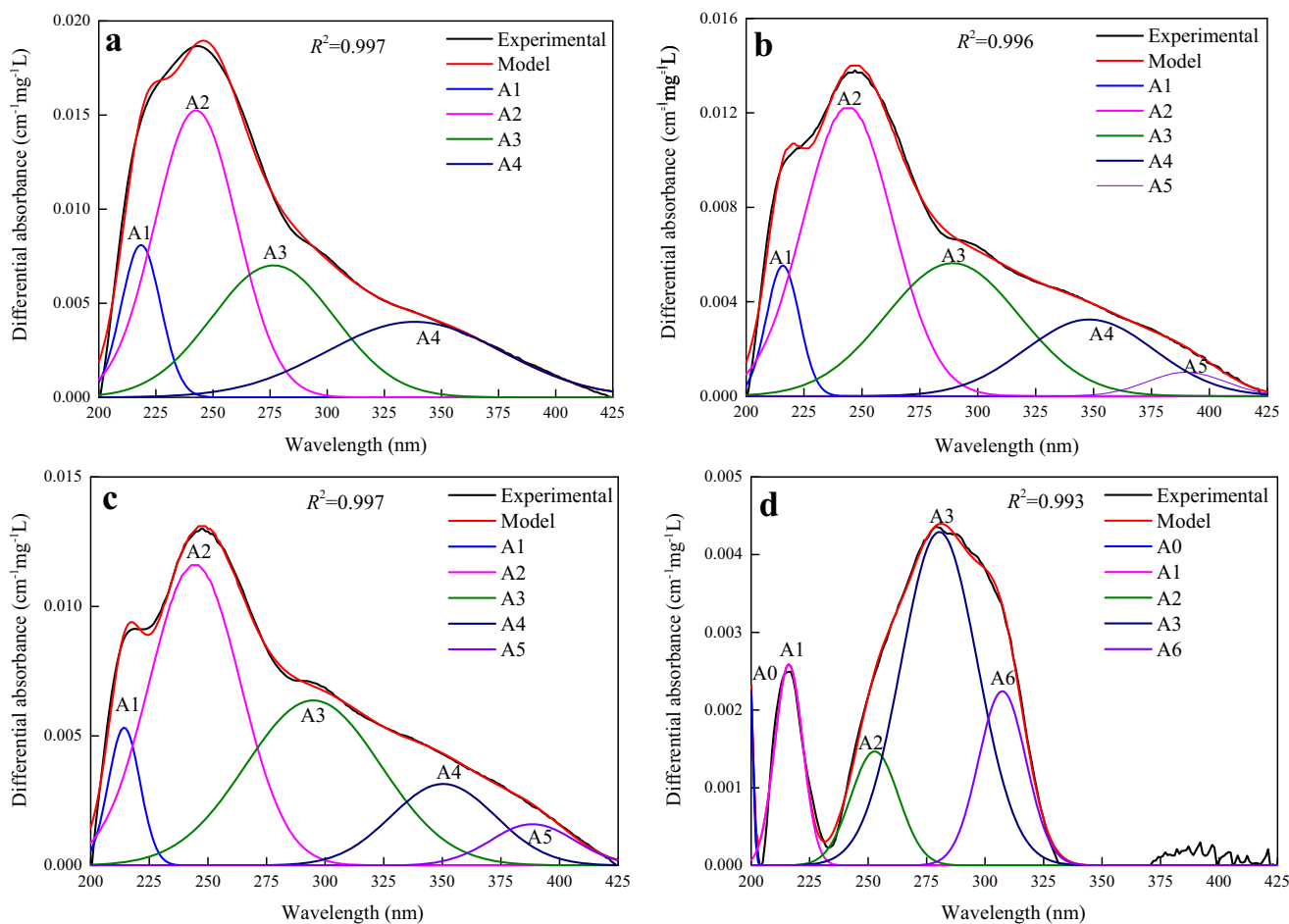
Fig. 2 Gaussian band fitting of DAS of interest FA subfractions (**a** FA_3; **b** FA_5; **c** FA_7; **d** FA_9)

in BESF than others. The same functional groups were also observed in differential spectra of Suwannee River fulvic acid during quenching by copper titration (Yan et al. 2013a). The eluting-dependent DAS combined with the Gaussian model made it possible to show the notable features for dynamic changes for FA subfractions by distinguishing the presence

and contributions of distinct bands to overall DAS shape. The DAS–Gaussian model could help reveal more comprehensive information about various chromophores (e.g., salicylic-type groups and carboxyl groups) in DOM. Moreover, the DAS–Gaussian model could make absorbance spectra more feature rich and quantify the spectral evolution as

Table 1 Comparison of properties of the Gaussian bands of interest FA subfractions

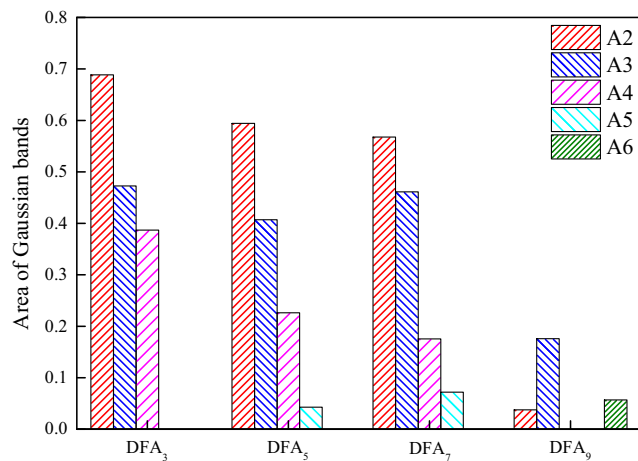| Gaussian bands	Interest FA subfractions	Position of maximum E_i (eV)	E_i standard deviation σ (eV)	Position of maximum E_i (nm)	E_i standard deviation σ (nm)	Bandwidth W_i (eV)	W_i standard deviation σ (nm)	Fit parameter (R^2)
A0	FA_9	6.20	–	200.00	–	1.16	–	0.993–0.997
A1	FA_3, FA_5, FA_7, FA_9	5.74	0.04	216.18	1.50	7.12	0.97	
A2	FA_3, FA_5, FA_7, FA_9	5.09	0.08	246.20	3.85	16.78	3.85	
A3	FA_3, FA_5, FA_7, FA_9	4.35	0.11	285.22	7.26	25.23	5.20	
A4	FA_3, FA_5, FA_7	3.59	0.06	345.64	5.30	29.50	6.72	
A5	FA_5, FA_7	3.19	0.01	389.27	0.79	17.43	0.52	
A6	FA_9	4.03	–	307.37	–	10.13	–	

Fig. 3 Areas of Gaussian bands for FA$_3$–FA$_9$

a function of any desired reaction parameter (e.g., metal complexation) (Yan et al. 2014).

Comparison and changes in the absorption spectral features with elution sequence

Seven spectral indices (i.e., SUVA$_{254}$, $A_{240–400}$, E_{300}/E_{400}, $S_{350–400}$, $\Delta A_{254}/A_{254}$, $\Delta S_{350–400}$, and ΔLnA_{350}) from the UV–Vis, LTAS, and DAS were used to assess the properties of FA subfractions. Previous literatures have reported that the greater SUVA$_{254}$ and $A_{240–400}$ indicated higher humification degree, molecular condensation, and aromaticity of DOM, respectively (He et al. 2011; Helms et al. 2008; Zhu et al. 2017). The values of SUVA$_{254}$ (2.70–3.31) and $A_{240–400}$ (22.70–26.40) of AESF were greater than the corresponding values of SUVA$_{254}$ (1.94–2.33) and $A_{240–400}$ (17.72–21.47) of NESF and BESF, respectively. These results indicated that the AESF might have higher humification degree, molecular condensation, and aromaticity than the NESF and BESF. These results might be attributed to the structural changes during the acidification, purification, and stepwise elution processes for the isolation and fractionation of soil FA. The reasons and mechanisms for these phenomena need to be further explored in a future study. However, the $S_{350–400}$ values (0.01413–0.017) of AESF were slightly lower than those (0.01743–0.01928) of NESF and BESF. Moreover, greater E_{300}/E_{400} values of DOM were associated with lower molecular weight and polymerization (Artinger et al. 2000; He et al. 2016; Zhu et al. 2017). The E_{300}/E_{400} values of AESF (4.00–4.75) were lower than those (5.11–7.43) of both NESF and BESF, suggesting that greater molecular mass and polymerization were presented for AESF. The larger molecular mass for AESF was also measured by size exclusion chromatography (Bai et al. 2015). The values of $\Delta A_{254}/A_{254}$ (0.28–0.41) of both DFA$_3$ and DFA$_5$ were larger than those (0.11–0.17) of both DFA$_7$ and DFA$_9$ (Fig. S1). Previous researchers have identified that the greater values of $\Delta A_{254}/A_{254}$ indicated higher hydroxyl radical production of organic species (Gerrity

et al. 2012; Nanaboina and Korshin 2010). The $\Delta S_{350–400}$ value of DFA$_3$ and DFA$_5$ (0.0023–0.0052) was slightly greater than those (0.0014–0.0019) of DFA$_3$, DFA$_7$, and DFA$_9$ (Fig. S1). The ΔLnA_{350} values of both DFA$_3$ and DFA$_5$ ranged 0.29–0.38, while the ΔLnA_{350} values from both DFA$_7$ and DFA$_9$ were near zero (Fig. S1). The $\Delta S_{350–400}$ and ΔLnA_{350} of DOM had positive correlations with salicylic-like and DOM–metal-bound functional groups, respectively (Li and Hur 2017; Yan et al. 2016). Therefore, the AESF had more hydroxyl radical production and salicylic-like and DOM–metal-bound functional groups. These phenomenon might be attributed to the protonation/deprotonation of FA with stepwise elution by different buffer pH values, which affected the molecular structure, configuration, conformation, intramolecular reaction, and functional group properties of FA (Dryer et al. 2008).

D-EEMs and fluorescence spectral features of FA subfractions

The D-EEMs could provide detailed information of the compositions and fluorescent components by eliminating the effect of nonreactive matters (Chen et al. 2003; Zhou et al. 2013). The D-EEMs of interest FA subfractions (i.e., FA$_3$–FA$_9$) with FA$_{13}$ as reference were established to explore their dynamic variations with the elution sequence (Fig. 4). In the D-EEMs of FA$_3$–FA$_9$, four main peaks named as peaks A–D were identified, and the spectral parameters of the D-EEMs of FA$_3$–FA$_9$ were shown (Table 2). In detail, for the D-EEMs of FA$_3$–FA$_7$, two main negative peaks were observed at Ex/Em of 215–220/300–315 nm (peak A) and 270–275/300–310 nm (peak B) (Fig. 4, Table 2). In addition, for the D-EEMs of FA$_9$, there are two main positive peaks at Ex/Em of 216/300 nm (peak A) and 272/304 nm (peak B) (Fig. 4, Table 2). One positive peak at Ex/Em of 255–265/420–450 nm (Peak C) appeared in the D-EEMs of FA$_3$–FA$_7$ (Fig. 4, Table 2). Moreover, one positive peak at Ex/Em of 312/442 nm (peak D) was only observed in the D-EEMs of FA$_3$ (Fig. 4, Table 2). Peaks A–D in D-EEMs could be assigned to tyrosine-like, tryptophan-like, fulvic-like, and humic-like materials, respectively (Chen et al. 2003; Wei et al. 2016; Zhou et al. 2013). In the D-EEMs, the negative fluorescence intensities of peak A ranged from ~ 171.0 to ~ 135.2 a.u., while the negative intensities of peak B ranged from ~ 221.6 to ~160.7 a.u. (Fig. 5, Table 2). The positive fluorescence intensities of peak A and peak B in D-EEMs of FA$_9$ were 244.0 and 262.5 a.u., respectively (Fig. 5, Table 2). These differences of peak A and peak B suggested that more tyrosine-like and tryptophan-like materials were eluted and concentrated in FA$_9$ by alkaline elution buffers. It was because that the protein-like materials were hydrophilic by ionization, resulting in the desorbing from XAD-8 via electrostatic repulsion at basic pH range (Bai et al. 2015). The fluorescence intensity of peak C (289.9 a.u.) of FA$_3$ was much greater than those (103.9–
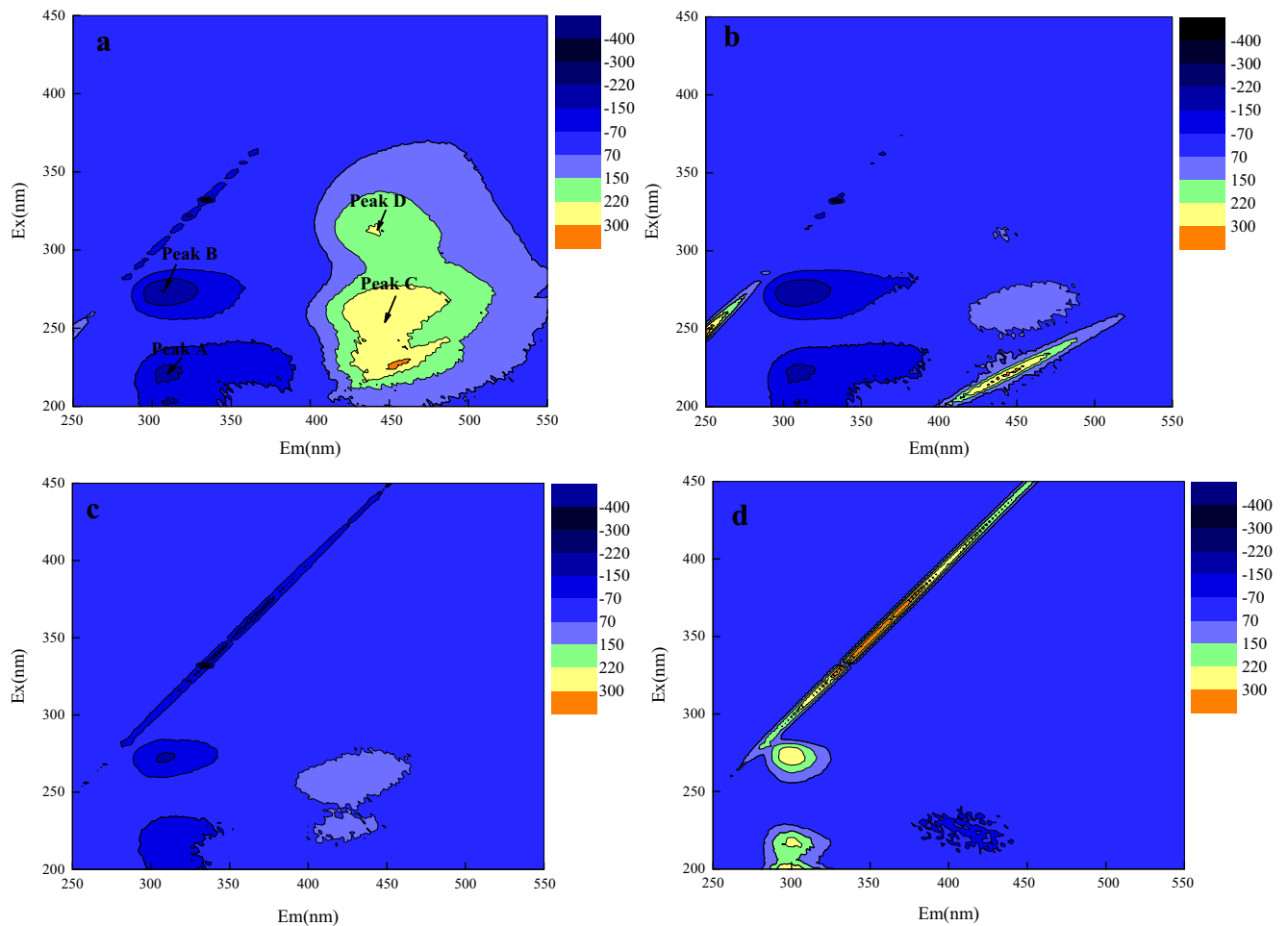
Fig. 4 D-EEMs of the interest FA subfractions (**a** FA_3; **b** FA_5; **c** FA_7; **d** FA_9)

Table 2 Spectral properties of fluorescence peaks in D-EEMs of interest FA subfractions (FA_3–FA_9)

| Peaks	Interest FA subfractions	Peak locations (Ex/Em nm)	Intensity (a.u.)	Category
Peak A	FA_3	220/311	-171.0	Tyrosine-like materials
	FA_5	220/310	-178.2	Tyrosine-like materials
	FA_7	220/310	-135.2	Tyrosine-like materials
	FA_9	216/300	244.0	Tyrosine-like materials
Peak B	FA_3	274/306	-221.6	Tryptophan-like materials
	FA_5	274/310	-217.6	Tryptophan-like materials
	FA_7	272/308	-160.7	Tryptophan-like materials
	FA_9	272/304	262.5	Tryptophan-like materials
Peak C	FA_3	262/448	289.9	Fulvic-like materials
	FA_5	264/442	103.9	Fulvic-like materials
	FA_7	258/422	118.7	Fulvic-like materials
	FA_9	–	–	–
Peak D	FA_3	312/442	224.1	Humic-like materials
	FA_5	–	–	–
	FA_7	–	–	–
	FA_9	–	–	–

– data not available
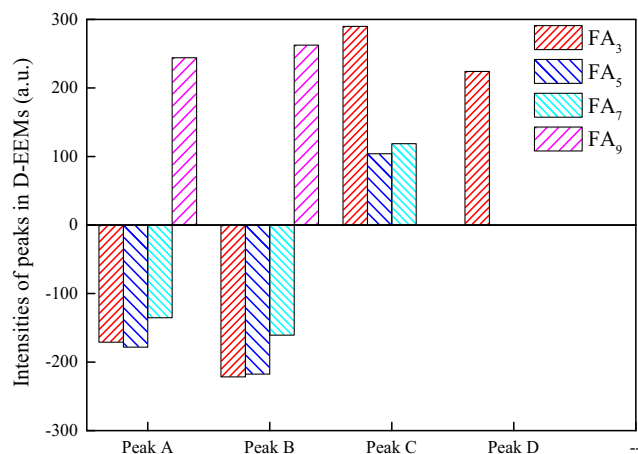
Fig. 5 Fluorescence intensities of peaks in D-EEMs of FA_3–FA_9

118.7 a.u.) of both FA_5 and FA_7, as well as that with about zero of FA_9 in D-EEMs (Fig. 5, Table 2). Additionally, peak D, related to humic-like materials, only appeared in D-EEMs of FA_3 with fluorescence intensity of 224.1 a.u. (Fig. 5, Table 2). Therefore, the fulvic-like and humic-like materials were dominant in FA_3, and the fulvic-like materials in FA subfractions decreased with elution sequence. By eliminating the fluorescence of nonreactive matters in EEMs in FA subfractions, therefore, the subtle changes of fluorescence spectra were highlighted by DFS, allowing the examination and comparison of the eluting-dependent fluorophores and fluorescence indices.

Four alternative fluorescence indices (i.e., AFI/UV, FI, BI, and HIX) derived from EEMs were proposed for assessing the fluorescent quantum yield, aromaticity, terrigenous contribution, and humic character of FA subfractions, respectively (Birdwell and Engel 2010; Xiao et al. 2016). The values of FI and BI of FA subfractions ranged 1.12–1.35 and 0.25–0.61, respectively, which were comparable to the corresponding values of FI (0.8–1.4) and BI (0.3–0.78) of soil-derived

DOM (Birdwell and Engel 2010). The values of FI (1.27–1.35) and BI (0.46–0.61) of both NESF and BESF were greater than the corresponding values of FI (1.12–1.15) and BI (0.25–0.32) of AESF, which suggested that the AESF had greater aromaticity than NESF and BESF. According to a previous study, it was consistent that the AESF contained more conjugated aromatic structures and less N-containing groups than both NESF and BESF by determining the elemental compositions of FA subfractions (Bai et al. 2015). The AFI/UV values (5.83–6.01) of both FA_5 and FA_9 were slightly smaller than those (6.56–7.23) of FA_3, FA_7, and FA_{13}, indicating that the FA_5 and FA_9 had higher fluorescent quantum yields that were associated to the π-conjugated systems with more polycyclic aromatic structures (Ohno et al. 2008; Xiao et al. 2016). The different results from AFI/UV and other indices (e.g., FI and BI) might be because the n–$π^*$ electronic transitions associated with AFI/UV values were affected by different contents of $-NH_3^+$, $-COOH$, and other electron-deficient groups in FA subfractions (Xiao et al. 2016). The possible mechanisms for this phenomenon should be investigated in the future.

The HIX has been widely utilized to compare the humic characters and terrigenous contributions of DOM (Birdwell and Engel 2010; Zsolnay et al. 1999). Different HIX values corresponded to the DOM with strong humic character/important terrigenous contribution (HIX > 10), important humic character, and weak recent autochthonous component (HIX 6–10), weak humic character and important recent autochthonous component (HIX 4–6), and biological or aquatic bacterial origin (HIX 0–4) (Huguet et al. 2010). The HIX values of FA subfractions ranged from 2.43 to 34.37, showing various humic characters and terrigenous contributions. In detail, the HIX values (21.46–34.37) for AESF were much greater than those (2.43–7.68) for both NESF and BESF, indicating that the AESF had stronger humic characters and more important terrigenous contributions than NESF and BESF. These
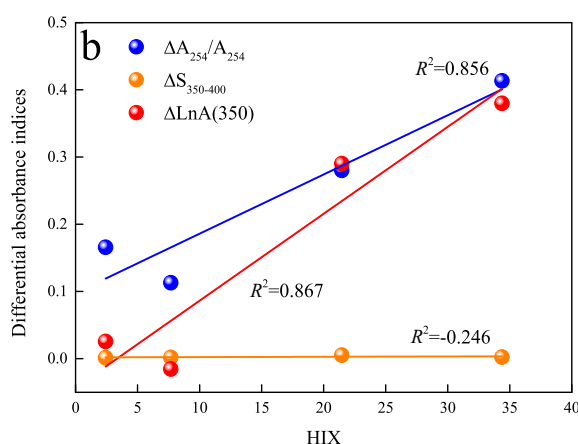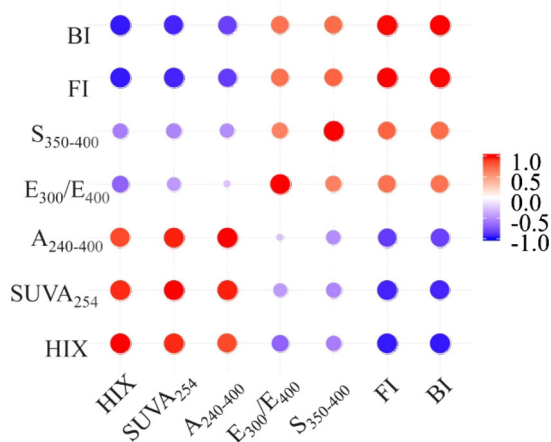

Fig. 6 Correlation analyses between humification indices and specific indices from absorption and fluorescence spectra of FA_3–FA_{13} (a) and FA_3–FA_9 (b) subfractions

results were consistent with the analysis of $SUVA_{254}$ of FA subfractions as discussed above. Additionally, the HIX value of FA_7 was 7.68, suggesting that the FA_7 had important humic character and weak recent autochthonous component. The lower HIX values (2.43–3.54) of BESF were comparable to those (1.21–3.92) of DOM derived from fresh organic matter, such as plant biomass and animal waste (Jian et al. 2016; Mielnik and Kowalczuk 2018).

Relationships among the selected spectral indices

The absorbance index $SUVA_{254}$ and the fluorescence index HIX were the most common indices to investigate the humification degree of DOM derived from soil or water environments (Birdwell and Engel 2010; Birdwell and Valsaraj 2010). Based on the UV–Vis, LTAS, and EEM data of FA subfractions, the correlation analyses between humification indices (i.e., $SUVA_{254}$ and HIX) and specific indices (i.e., $S_{350-400}$, $A_{240-400}$, E_{300}/E_{400}, $\Delta A_{254}/A_{254}$, $\Delta S_{350-400}$, $\Delta LnA(350)$, FI, and BI) were shown (Fig. 6, S2 and Table 3). Both $SUVA_{254}$ and HIX were significant negatively correlated with both FI and BI ($p < 0.05$) (Fig. 6a and Table 3). However, both $SUVA_{254}$ and HIX exhibited weak correlations with E_{300}/E_{400}, $S_{350-400}$, and $\Delta S_{350-400}$ (Fig. 6a and Table 3). Additionally, the $SUVA_{254}$ exhibited a significant positive correlation with $A_{240-400}$ ($p < 0.01$) (Fig. 6a and Table 3). These results suggested that the humification degree of FA subfractions was closely related to their aromaticity, conjugated aromatic structures, and molecular condensation, rather than their molecular weight and polymerization. For the specific indices from DAS, both $SUVA_{254}$ and HIX were significant positively correlated with $\Delta A_{254}/A_{254}$ ($R^2 = 0.856-0.982$) and $\Delta LnA(350)$ ($R^2 = 0.867-0.992$) (Figs. 6b and S2, Table 3). These results indicated that the DOM–metal-bound

functional groups (e.g., carboxyl and phenolic groups) were also closely associated to the humification degree of FA subfractions. According to the carbon distributions of FA subfractions from ^{13}C NMR spectroscopy in our recent study, both phenolic and carboxylic carbon showed significant correlations with $SUVA_{254}$ and HIX ($R^2 = 0.676-0.882$) (Fig. S3). Meanwhile, the significant correlations between the hydroxyl radical production and humification degree for FA subfractions need further studied. The selected spectral indices derived from differential spectroscopy were beneficial for comparing the differences in structural or functional properties (e.g., aromaticity and humification) during the FA fractionation process. In addition, the suitable spectral indices could also help perform online and real-time monitoring of environmental behaviors of DOM in the future, such as the property changes under the interference of external environmental factors.

Conclusions

The LTAS and DAS of FA subfractions exhibited different features (i.e., spectral slope and differential peaks) due to emerging variations of different chromophores and molecule conformations with stepwise elution. With the DAS–Gaussian fitting deconvolution, the DFA_3–DFA_9 comprised seven different Gaussian bands (A0–A6). The intensities, widths, and areas of Gaussian bands existed differences among FA subfractions ($R^2 > 0.993$). The content of salicylic-like and carboxyl groups in FA subfractions decreased, while the content of phenolic chromophore increased with elution sequence according to Gaussian band areas. AESF had higher molecular weight/condensation, polymerization, hydroxyl radical production, humification degree, and terrigenous contribution,

Table 3 Pearson rank order correlations of various indices for FA subfractions

Indicators	$SUVA_{254}$	$S_{350-400}$	E_{300}/E_{400}	$A_{240-400}$	$\Delta A_{254}/A_{254}$	$\Delta S_{350-400}$	$\Delta LnA(350)$	FI	BI	HIX
$SUVA_{254}$	1	−0.528	−0.434	0.966**	0.994**	0.253	0.945	−0.925*	−0.923*	0.950*
$S_{350-400}$		1	−0.631	−0.493	−0.338	1.000**	−0.556	0.766	0.730	−0.556
E_{300}/E_{400}			1	−0.257	−0.476	−0.733	−0.629	0.700	0.702	−0.675
$A_{240-400}$				1	0.963*	0.227	0.901	−0.841	−0.819	0.863
$\Delta A_{254}/A_{254}$					1	0.338	0.970*	−0.901	−0.886	0.950*
$\Delta S_{350-400}$						1	0.556	−0.617	−0547	0.412
$\Delta LnA(350)$							1	−0.964*	−0.935	0.955*
FI								1	0.995**	−0.954*
BI									1	−0.955*
HIX										1

*Correlation is significant at the 0.05 level (2-tailed)

**Correlation is significant at the 0.01 level (2-tailed)

as well as contained more conjugated aromatic structures and less N-containing groups than NESF and BESF based on the spectral indices analysis. Based on the correlations of spectral indices of FA subfractions, the humification degree might be related to the aromaticity, molecular condensation, and DOM–metal-bound functional groups of DOM. The novel differential spectroscopy and comprehensive spectral indicators in this study can effectively help us unearth the mystery of heterogeneous binding processes and complex interaction mechanisms of DOM with various environmental contaminants in the further study.

References

Albrecht R, Le Petit J, Terrom G, Perissol C (2011) Comparison between UV spectroscopy and Nirs to assess humification process during sewage sludge and green wastes co-composting. Bioresour Technol 102(6):4495–4500

Artinger R, Buckau G, Geyer S, Fritz P, Wolf M, Kim JI (2000) Characterization of groundwater humic substances: influence of sedimentary organic carbon. Appl Geochem 15(1):97–116

Bai Y, Wu F, Xing B, Meng W, Shi G, Ma Y, Giesy JP (2015) Isolation and characterization of Chinese standard fulvic acid sub-fractions separated from forest soil by stepwise elution with pyrophosphate buffer. Sci Rep 5:8723

Birdwell JE, Engel AS (2010) Characterization of dissolved organic matter in cave and spring waters using UV–Vis absorbance and fluorescence spectroscopy. Org Geochem 41(3):270–280

Birdwell JE, Valsaraj KT (2010) Characterization of dissolved organic matter in fogwater by excitation-emission matrix fluorescence spectroscopy. Atmos Environ 44(27):3246–3253

Chen H, Kenny JE (2012) Application of PARAFAC to a two-component system exhibiting fluorescence resonance energy transfer: from theoretical prediction to experimental validation. Analyst 137(1):153–162

Chen W, Westerhoff P, Leenheer JA, Booksh K (2003) Fluorescence excitation-emission matrix regional integration to quantify spectra for dissolved organic matter. Environ Sci Technol 37(24):5701–5710

Chen Y, Fabbricino M, Luongo V, Korshin GV (2019) Differential absorbance study of interactions between europium, soil and aquatic NOM and model compounds. Chemosphere 235:96–103

Dai J, Ran W, Xing B, Gu M, Wang L (2006) Characterization of fulvic acid fractions obtained by sequential extractions with pH buffers, water, and ethanol from paddy soils. Geoderma 135(11):284–295

Dryer DJ, Korshin GV, Fabbricino M (2008) In situ examination of the protonation behavior of fulvic acids using differential absorbance spectroscopy. Environ Sci Technol 42(17):6644–6649

Fu P Q. (2014) Dissolved organic matter in naturalaquatic environments and its complexation with metal ions: a study based on fluorescence spectroscopy (in Chinese, doctoral dissertation, Guiyang: Institute of Geochemistry, Chinese Academy of Sciences)

Fuentes M, González-Gaitano G, García-Mina JM (2006) The usefulness of UV–visible and fluorescence spectroscopies to study the chemical nature of humic substances from soils and composts. Org Geochem 37(12):1949–1959

Gao Y, Yan M, Korshin GV (2015a) Effects of calcium on the chromophores of dissolved organic matter and their interactions with copper. Water Res 81:47–53

Gao Y, Yan M, Korshin GV (2015b) Effects of ionic strength on the chromophores of dissolved organic matter. Environ Sci Technol 49(10):5905

Gerrity D, Gamage S, Jones D, Korshin GV, Lee Y, Pisarenko A, Trenholm RA, Gunten UV, Wert EC, Snyder SA (2012) Development of surrogate correlation models to predict trace organic contaminant oxidation and microbial inactivation during ozonation. Water Res 46(19):6257–6272

He X, Xi B, Wei Z, Guo X, Li M, An D, Liu H (2011) Spectroscopic characterization of water extractable organic matter during composting of municipal solid waste. Chemosphere 82(4):541–548

He W, Lee JH, Hur J (2016) Anthropogenic signature of sediment organic matter probed by UV-visible and fluorescence spectroscopy and the association with heavy metal enrichment. Chemosphere 150:184–193

Helms JR, Stubbins A, Ritchie JD, Minor EC, Kieber DJ, Mopper K (2008) Absorption spectral slopes and slope ratios as indicators of molecular weight, source, and photobleaching of chromophoric dissolved organic matter. Limnol Oceanogr 53(3):955–969

Huguet A, Vacher L, Relexans S, Saubusse S, Froidefond JM, Parlanti E (2009) Properties of fluorescent dissolved organic matter in the Gironde estuary. Org Geochem 40(6):706–719

Huguet A, Vacher L, Saubusse S, Etcheber H, Abril G, Relexans S, Ibalot F, Parlanti E (2010) New insights into the size distribution of fluorescent dissolved organic matter in estuarine waters. Org Geochem 41(6):595–610

Janot N, Reiller PE, Korshin GV, Benedetti MF (2010) Using spectrophotometric titrations to characterize humic acid reactivity at environmental concentrations. Environ Sci Technol 44(17):6782–6788

Jian S, Liang G, Li Q, Zhao Y, Gao M, She Z, Jin C (2016) Three-dimensional fluorescence excitation–emission matrix (EEM) spectroscopy with regional integration analysis for assessing waste sludge hydrolysis at different pretreated temperatures. Environ Sci Pollut Res Int 23(23):1–7

Kalbitz K, Geyer W, Geyer S (1999) Spectroscopic properties of dissolved humic substances: a reflection of land use history in a fen area. Biogeochemistry 47(2):219–238

Li P, Hur J (2017) Utilization of UV-Vis spectroscopy and related data analyses for dissolved organic matter (DOM) studies: a review. Crit Rev Env Sci Tec 47(3):131–154

Li T, Song F, Zhang J, Liu S, Xing B, Bai Y (2020a) Pyrolysis characteristics of soil humic substances using TG-FTIR-MS combined with kinetic models. Sci Total Environ 698:134237

Li T, Song F, Zhang J, Tian S, Huang N, Xing B, Bai Y (2020b) Experimental and modeling study of proton and copper binding properties onto fulvic acid fractions using spectroscopic techniques combined with two-dimensional correlation analysis. Environ Pollut 256:113465. https://doi.org/10.1016/j.envpol.2019.113465

Mcknight DM, Boyer EW, Westerhoff PK, Doran PT, Kulbe T, Andersen DT (2001) Spectrofluorometric characterization of dissolved organic matter for indication of precursor organic material and aromaticity. Limnol Oceanogr 46(1):38–48

Miao S, Lyu H, Wang Q, Li Y, Wu Z, Du C, Xu J, Bi S, Mu M, Lei S (2019) Estimation of terrestrial humic-like substances in inland lakes based on the optical and fluorescence characteristics of chromophoric dissolved organic matter (CDOM) using OLCI images. Ecol Indic 101:399–409

Mielnik L, Kowalczuk P (2018) Optical characteristic of humic acids from lake sediments by excitation-emission matrix fluorescence with PARAFAC model. J Soils Sediments:1–12

Mobed JJ, Hemmingsen SL, Autry JL, McGown LB (1996) Fluorescence characterization of IHSS humic substances: total luminescence spectra with absorbance correction. Environ Sci Technol. 30(10):3061–3065

Nanaboina V, Korshin GV (2010) Evolution of absorbance spectra of ozonated wastewater and its relationship with the degradation of trace-level organic species. Environ Sci Technol 44(16):6130–6137

Ohno T, Chorover J, Omoike A, Hunt J (2007) Molecular weight and humification index as predictors of adsorption for plant- and manure-derived dissolved organic matter to goethite. Eur J Soil Sci 58(1):125–132

Ohno T, Wang Z, Bro R (2008) PowerSlicing to determine fluorescence lifetimes of water-soluble organic matter derived from soils, plant biomass, and animal manures. Anal Bioanal Chem 390(8):2189–2194

Pan H, Yu H, Song Y, Liu R, Du E (2017) Application of solid surface fluorescence EEM spectroscopy for tracking organic matter quality of native halophyte and furrow-irrigated soils. Ecol Indic 73:88–95

Parker CA, Rees WT (1960) Correction of fluorescence spectra and measurement of fluorescence quantum efficiency. Analyst 85(1013):587–600

Peng N, Wang K, Liu G, Li F, Yao K, Lv W (2014) Quantifying interactions between propranolol and dissolved organic matter (DOM) from different sources using fluorescence spectroscopy. Environ Sci Pollut Res Int 21(7):5217–5226

Praise S, Ito H, An Y, Watanabe K, Watanabe T (2018) Dissolved organic matter characteristics along sabo dammed streams based on ultraviolet visible and fluorescence spectral properties. Environ Monit Assess 190(3):146

Song F, Wu F, Guo F, Wang H, Feng W, Zhou M, Deng Y, Bai Y, Xing B, Giesy JP (2017a) Interactions between stepwise-eluted sub-fractions of fulvic acids and protons revealed by fluorescence titration combined with EEM-PARAFAC. Sci Total Environ 605-606:58–65

Song F, Wu F, Xing B, Li T, Feng W, Giesy JP, Guo W, Wang H, Liu S, Bai Y (2017b) Protonation-dependent heterogeneity in fluorescent binding sites in sub-fractions of fulvic acid using principle component analysis and two-dimensional correlation spectroscopy. Sci Total Environ 616–617:1279–1287

Song F, Wu F, Feng W, Tang Z, Giesy JP, Guo F, Shi D, Liu X, Qin N, Xing B, Bai Y (2018) Fluorescence regional integration and differential fluorescence spectroscopy for analysis of structural characteristics and proton binding properties of fulvic acid sub-fractions. J Environ Sci 74:116–125

Song F, Li T, Zhang J, Wang X, Bai Y, Giesy JP, Xing B, Wu F (2019a) Novel insights into the kinetics, evolved gases, and mechanisms for biomass (sugar cane residue) pyrolysis. Environ Sci Technol 53(22):13495–13505

Song F, Wu F, Feng W, Liu S, He J, Li T, Zhang J, Wu A, Amarasiriwardena D, Xing B, Bai Y (2019b) Fluorescence regional integration and differential fluorescence spectroscopy for analysis of structural characteristics and proton binding properties of fulvic acid sub-fractions. Chemosphere 74:116–125

Wei Z, Wang X, Zhao X, Xi B, Wei Y, Zhang X, Zhao Y (2016) Fluorescence characteristics of molecular weight fractions of dissolved organic matter derived from composts. Int Biodeterior Biodegradation 113:187–194

Xiao K, Sun J, Shen Y, Liang S, Liang P, Wang X, Huang X (2016) Fluorescence properties of dissolved organic matter as a function of hydrophobicity and molecular weight: case studies from two

membrane bioreactors and an oxidation ditch. RSC Adv 6(29):24050–24059

Xu H, Guan DX, Zou L, Lin H, Guo L (2018a) Contrasting effects of photochemical and microbial degradation on Cu(II) binding with fluorescent DOM from different origins. Environ Pollut 239:205

Xu H, Yan M, Li W, Jiang H, Guo L (2018b) Dissolved organic matter binding with Pb(II) as characterized by differential spectra and 2D UV–FTIR heterospectral correlation analysis. Water Res 144:435–443

Yan M, Korshin GV (2014) Comparative examination of effects of binding of different metals on chromophores of dissolved organic matter. Environ Sci Technol 48(6):3177–3185

Yan M, Dryer D, Korshin GV, Benedetti MF (2013a) In situ study of binding of copper by fulvic acid: comparison of differential absorbance data and model predictions. Water Res 47(2):588–596

Yan M, Fu Q, Li D, Gao G, Wang D (2013b) Study of the pH influence on the optical properties of dissolved organic matter using fluorescence excitation–emission matrix and parallel factor analysis. J Lumin 142(1):103–109

Yan M, Wang D, Korshin GV, Benedetti MF (2013c) Quantifying metal ions binding onto dissolved organic matter using log-transformed absorbance spectra. Water Res 47(7):2603–2611

Yan M, Korshin GV, Claret F, Croué J-P, Fabbricino M, Gallard H, Schafer T, Benedetti MF (2014) Effects of charging on the chromophores of dissolved organic matter from the Rio Negro basin. Water Res 59:154–164

Yan M, Lu Y, Gao Y, Benedetti MF, Korshin GV (2015) In-situ investigation of interactions between magnesium ion and natural organic matter. Environ Sci Technol 49(14):8323–8329

Yan M, Ma J, Ji G (2016) Examination of effects of Cu(II) and Cr(III) on Al(III) binding by dissolved organic matter using absorbance spectroscopy. Water Res 93:84–90

Yu GH, Luo YH, Wu MJ, Tang Z, Liu DY, Yang XM, Shen QR (2010) PARAFAC modeling of fluorescence excitation-emission spectra for rapid assessment of compost maturity. Bioresour Technol 101(21):8244–8251

Yu H, Xi B, Ma W, Li D, He X (2011) Fluorescence spectroscopic properties of dissolved fulvic acids from salined flavo-aquic soils around Wuliangsuhai in Hetao Irrigation District, China. Soil Sci Soc Am J 75(4):1385

Yue Z, Wei Y, Yun Z, Xin W, Xi B, Zhao X, Xu Z, Wei Z (2017) Roles of composts in soil based on the assessment of humification degree of fulvic acids. Ecol Indic 72:473–480

Zhang Y, Su Y, Liu Z, Yu J, Jin M (2017) Lipid biomarker evidence for determining the origin and distribution of organic matter in surface sediments of Lake Taihu, eastern China. Ecol Indic 77:397–408

Zhou J, Wang JJ, Baudon A, Chow AT (2013) Improved fluorescence excitation-emission matrix regional integration to quantify spectra for fluorescent dissolved organic matter. J Environ Qual 42(3):925–930

Zhu Y, Song Y, Yu H, Liu R, Liu L, Lv C (2017) Characterization of dissolved organic matter in Dongjianghu Lake by UV-visible absorption spectroscopy with multivariate analysis. Environ Monit Assess 189(9):443

Zsolnay A, Baigar E, Jimenez M, Steinweg B, Saccomandi F (1999) Differentiating with fluorescence spectroscopy the sources of dissolved organic matter in soils subjected to drying. Chemosphere 38(1):45–50

Investigation of eluted characteristics of fulvic acids using differential spectroscopy combined with Gaussian deconvolution and spectral indices

Tingting Li[1#], Fanhao Song[1,2#], Jin Zhang[3], Shasha Liu[1], Weiying Feng[1], Lingling Zuo[4], Jia Pu[2], Baoshan Xing[5], John P. Giesy[1,6], Yingchen Bai[1]*

[1]State Key Laboratory of Environmental Criteria and Risk Assessment, Chinese Research Academy of Environmental Science, Beijing, 10012, China

[2]College of Water Sciences, Beijing Normal University, Beijing, 100875, China

[3]School of Environmental and Safety Engineering, Changzhou University, Jiangsu, 213164, China

[4]School of Management, China University of Mining and Technology, Beijing, 221116, China

[5]Stockbridge School of Agriculture, University of Massachusetts, Amherst, MA, 01003, USA

[6]Department of Biomedical and Veterinary Biosciences and Toxicology Centre, University of Saskatchewan, Saskatoon, Saskatchewan, SK, S7N 5B3, Canada

Number of Pages (including this cover sheet): 6

Number of Figs.: 4

#Tingting Li and Fanhao Song contributed equally to this work.

*Corresponding author: Tel.: +86-10-84931804; Fax: +86-10-84931804.
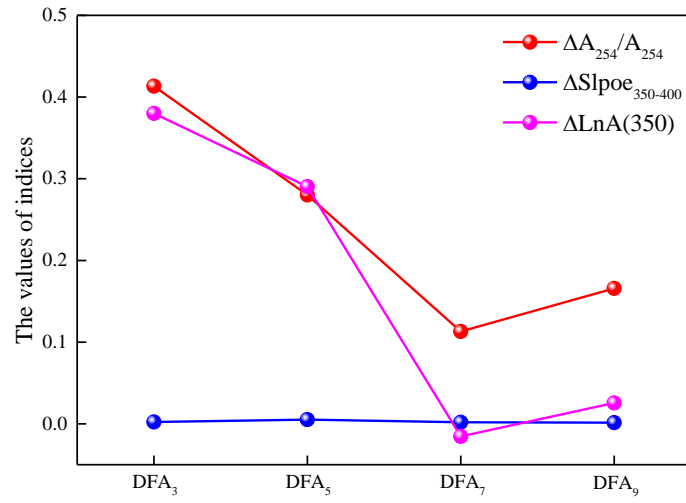
E-mail: baiyc@craes.org.cn.

31

32   **Fig. S1.** Specific indices from FA$_3$-FA$_9$.

33

Fig. S2. Correlations between $SUVA_{254}$ and specific indices ($\Delta A_{254}/A_{254}$, $\Delta S_{350-400}$,

$\Delta LnA(350)$) from FA_3-FA_9.

36

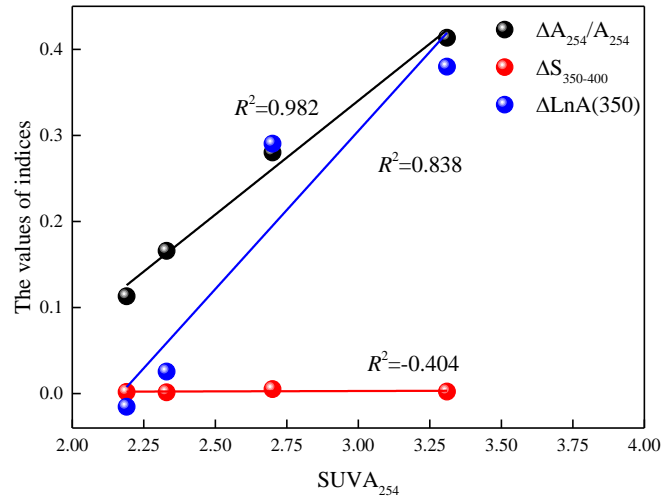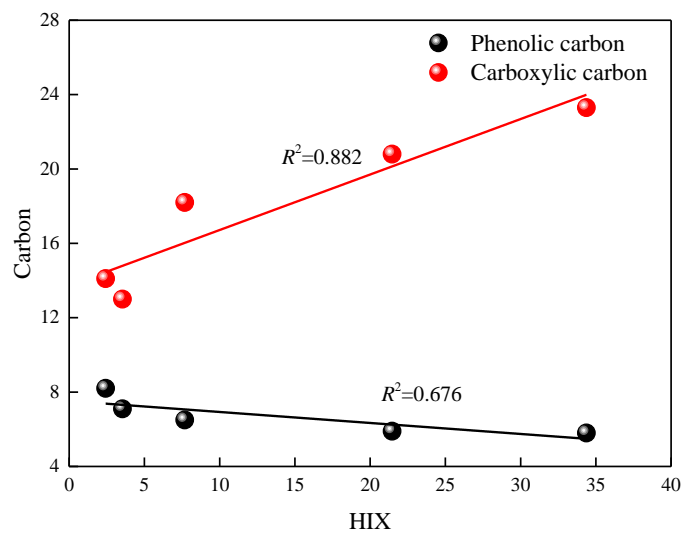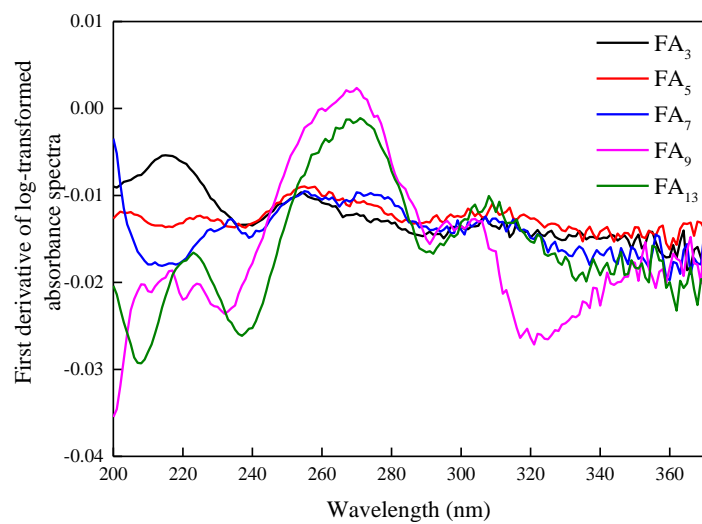37   **Fig. S3.** Correlations between HIX and phenolic/carboxylic carbon in FA sub-fractions.

38
39 **Fig. S4.** The first-order derivative of log-transformed absorbance spectra of FA sub-fraction.